Eur. Phys. J. B **6**, 183–193 (1998)

THE EUROPEAN PHYSICAL JOURNAL B

Light-induced bistability in spin transition solids leading to thermal and optical hysteresis

A. Desaix[1], O. Roubeau[1,2], J. Jeftic[1], J.G. Haasnoot[3], K. Boukheddaden[1], E. Codjovi[1], J. Linarès[1], M. Noguès[1], and F. Varret[1,a]

[1] Laboratoire de Magnétisme et d'Optique, CNRS-Université de Versailles, 45 avenue des États-Unis, 78035 Versailles Cedex, France
[2] Institut de Recherche sur la Réactivité, l'Électrochimie et la Microporosité, CNRS-Université de Versailles, 45 avenue des États-Unis, 78035 Versailles Cedex, France
[3] Leiden Institute of Chemistry, Gorlaeus Laboratories, Leiden University, P.O. Box 9502, 2300 RA Leiden, The Netherlands

Received: 5 June 1997 / Accepted: 17 July 1998

Abstract. We investigate the behaviour of photo-excitable, bistable systems, under permanent light irradiation, in presence of relaxation towards the non-excited state. Cooperativity causes bistability of the steady state, leading to light-induced thermal and optical hysteresis (LITH and LIOH). The light-induced instability is expected to induce demixtion, *i.e.* the coexistence of domains of the two stable steady states. Such effects are evidenced by magnetic and reflectivity measurements on the spin-crossover solid solution: $[Fe_xCo_{1-x}(btr)_2(NCS)_2] \cdot H_2O$, with $x = 0.3$, 0.5, 0.85. Experimental data are in quantitative agreement with a simple macroscopic model which includes a non-linear relaxation term in the master equation.

PACS. 64.60.My Metastable phases – 70.60.Es Relaxation effects – 75.90.+w Other topics in magnetic properties and materials – 78.20.Nv Thermooptical and photothermal effects

1 Introduction

Spin-crossover solids [1–4] are text-book examples of photo-excitable materials, which are studied for future applications as optical memories or numerical displays [5,6]. The optical switching is performed at low temperature, by the so-called direct or inverse LIESST effect (Light Induced Excited Spin State Trapping [7–10]), using different wavelengths for the back and forth processes. For most examples, the low- temperature stable state is low-spin (LS); whereas the high-spin state (HS) is thermodynamically favoured at high temperatures, due to the higher entropy. In presence of sufficient cooperativity, a first order LS-HS transition occurs, usually in the 100–400 K temperature range; it is denoted "spin transition" and may exhibit thermal hysteresis, up to $\sim$ 50 K wide [11,12].

At low-temperature the ground state is LS which has a strong optical absorption in the visible range, giving the material a purple or deep pink colour. By irradiating into a LS-state absorption band ($\sim$ 550 nm), or in a neighbouring metal-ligand charge transfer band, the molecules are switched to the metastable HS state, which absorbs in the near IR, and the material becomes transparent. The reverse LIESST effect is obtained with red ($\sim$ 800 nm) light [10].

The LS $\leftrightarrow$ HS switching is easily detected by magnetic measurements (for Fe^{II}, the spin states are 0, 2), or by optical reflectivity [12–15]. Here we use both techniques simultaneously, using a SQUID magnetometer equipped with a double-beam optical fiber and the apparatus for optical reflectivity described in reference [14]. The "optical signal" given in the present data is proportional to the ratio reflected/incident intensity. Such a coupled device enables the comparison, at the same time, of the bulk and surface properties of the material [15] ("surface" is associated here with the penetration depth of the light). A strong optical absorption leads to inhomogeneous excitation of the sample, by layers parallel to the surface, as already quoted in [10], and inferred from experimental inhomogeneous relaxation curves in [16]. To avoid such an inhomogeneous character of the experiment, we used thin samples and, following A. Hauser's advice, we did not use the band maximum of the $^1A_1 \rightarrow {}^1T_1$ transition (550 nm), but an edge of the same band, at 600 nm. We show in Figure 1 that the magnetic and optical signals are then reasonably correlated, for both the thermal transition (Fig. 1a) and the LIESST process (see Fig. 11). The small steps in the reflectivity curve are due to the discontinuous change of temperature. In Figure 1b the discrepancy between the reflectivity and magnetisation curves

[a] e-mail: fvarret@physique.uvsq.fr

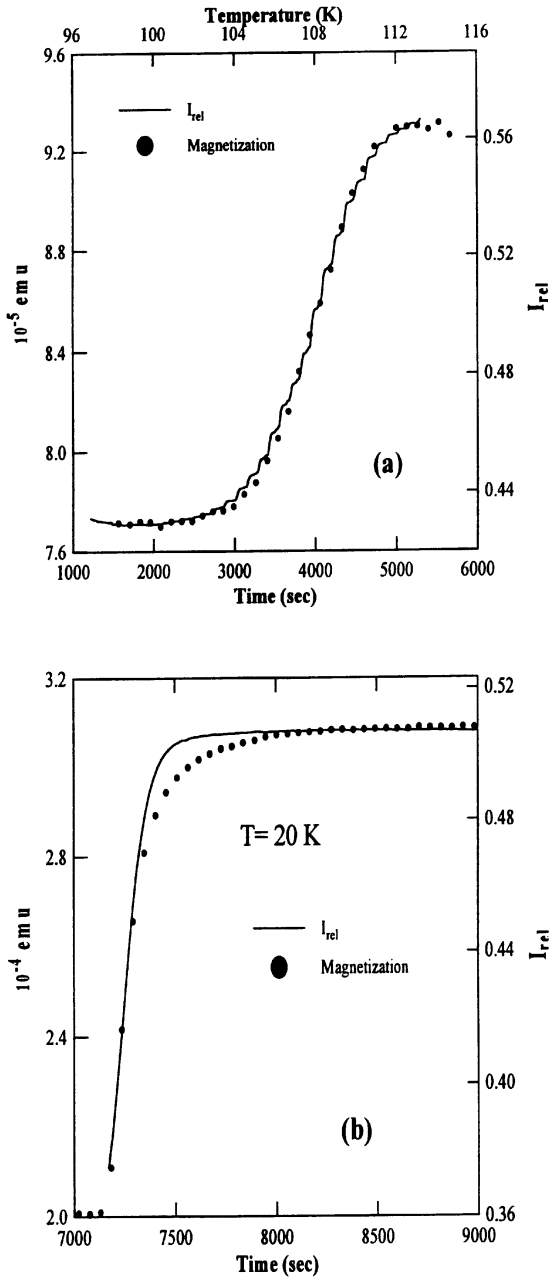

Fig. 1. Magnetic and optical signals of $[Fe_{0.5}Co_{0.5}(btr)_2(NCS)_2] \cdot H_2O$, under light irradiation of 600 nm, 40 mW/cm^2, at the thermal transition (a), and during photo-excitation at 20 K (b). The optical scale has been matched to the magnetic one.

is due to the complete photoexcitation of the "surface" prior to the one of the bulk.

High-temperature studies of the LIESST process are of interest in relation to the considerable efforts of the spin-crossover community for designing new materials with the highest operating temperature for optical switching. From that point of view, the mechanism which really may hinder or inhibit the photo-excitation process is the relaxation of the metastable, photo-excited molecular state. Such relaxation even occurs at low temperature, in the tunneling regime [16,17]. We consider here, for simplicity, a relaxation in the thermally activated region, in the temperature range where the photo-excitation and relaxation really compete, and finally result in a steady state with a partial excitation of the system. The initial goal of our investigations was to measure the relaxation rate through the steady state value, but the experiments turned out to reveal the bistability of the steady state, under chosen conditions of temperature, light-intensity and cooperativity strength.

The paper is organized as follows: a macroscopic model, describing the relaxation in the thermally activated region, is developped in Section 2, with respect to experimental data. The model is completed introducing the photoexcitation in Section 3, in terms of macroscopic master equation, from which the bistable character of the system is predicted. Experimental results are given in Section 4, with their quantitative analysis. Further consequences of the non-linear relaxation term are considered in Section 5: transient inhomogenous character of relaxation and demixtion under continuous irradiation. An intensity threshold effect is also discussed.

2 Relaxation: model and experiments

The effect of cooperativity on the relaxation rate of the metastable state has been evidenced by Hauser, Spiering and collaborators [18–20], from the non-exponential (sigmoidal) time dependence of the high-spin fraction, $n_{HS}(t)$, after photo-excitation. Experimental data above $\sim$ 40 K are consistent with a thermal activation process involving an energy barrier $E_a(n_{HS})$ depending linearly on n_{HS} [19]. Accordingly, the relaxation rate is written:

$$k_{HL}(T, n_{HS}) = k_\infty \exp\left(-\frac{E_a(n_{HS})}{kT}\right) \qquad (1)$$

or, using a self-acceleration factor $\alpha(T)$, proportional to the inverse temperature:

$$k_{HL}(T, n_{HS}) = k_\infty \exp\left(-\frac{E_a(0)}{kT}\right) \exp(-\alpha(T) n_{HS}). \quad (2)$$

The linear dependence $E_a(n_{HS})$, can be assigned to a quasi-linear variation of the electronic energy gap Δ with n_{HS} (see the configurational coordinate diagram sketched in Fig. 2), which exactly follows [22] the predictions of the mean-field Ising like model [22–25], and the equivalent Bragg-Williams approach of regular solutions [26–28]. Such a description has been spectacularly confirmed by pressure experiments [29,30] acting on Δ just as the order parameter n_{HS} does in the mean-field model. The description is also consistent with the elastic model of spin transitions [31,32].

Consequently, $\alpha(T)$ should be proportional to the cooperativity parameter, *e.g.* J in the Ising-like model. Further, the dilution of the spin-conversion element in a solid solution can be accounted for in the mean-field approach,

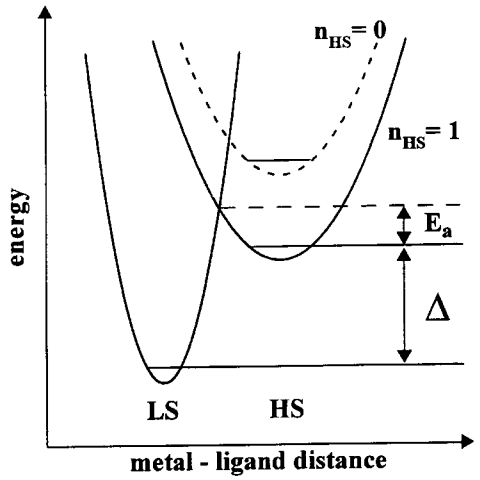

Fig. 2. Configurational coordinate diagram for a spin-crossover system, adapted from [3].

Table 1. Fitted values of the parameters involved in the decay of the metastable state, using equation (2). Experimental curves are presented in Figure 3.

x	T (K)	$k_{HL}(T, n_{HS} = 1/2)$ (10^{-3} s^{-1})	$\alpha(T, x)$	αT (K)	$\alpha T/x$ (K)
0.30	55	1.58	2.9	160	530
0.50	45	0.28	5.85	263	526
0.50	52	1.50	5.14	267	534
0.85	50	2.89	8.45	422	497

in the following simple way: $J_{eff} \sim x$, where x is the relative atomic concentration of the spin-crossover element. Then, the self-acceleration factor is written:

$$\alpha(T, x) = A\frac{x}{T} \tag{3}$$

where A is a constant depending on the nature (*i.e.* strength) of interactions and on the shape and position of the potential wells in the configurational coordinate diagram.

We show in Figure 3 typical relaxation curves recorded for samples with $x = 0.3, 0.5, 0.85$, whose sigmoidal shapes enable determination of α-values using equation (2).

The brief discussion of the relaxation curves and of the fitted data follows. The fits in Figure 3 were carried out so as to best account for the first half of the n_{HS} variation (approximately $n_{HS} > 0.5$); we have admitted a notable off-set between the fit and the experiment for the rest of the curve. This off-set is clearly increased with the increasing x. The effect has been recently analysed in terms of a progressive onset of correlations due to the short-range interactions [33]. In the present work, Section 5, we shall introduce an alternative (additional) mechanism in terms of transient inhomogeneity.

Fitted parameter values are listed in Table 1. The product $\alpha T/x$ is almost constant, as predicted by

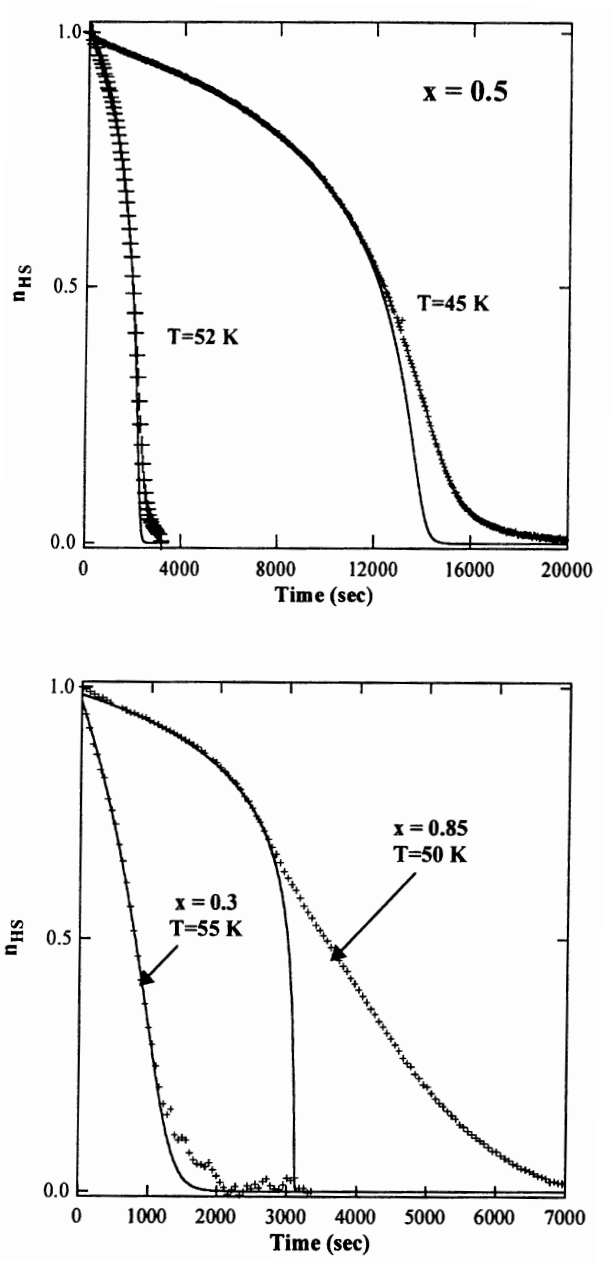

Fig. 3. Typical time dependences for the decay of the metastable state of $[Fe_xCo_{1-x}(btr)_2(NCS)_2] \cdot H_2O$. Solid lines are calculated according to equation (2). Fitted α-values are listed in Table 1. The misfits are discussed in the text.

equation (3). Using equation (2), the activation energy is estimated for $x = 0.5$, as $E_a(n_{HS} = 1/2) = 587$ K.

3 Theory

We now consider the effect of continuous irradiation of the sample in the temperature range where the HS $\rightarrow$ LS relaxation is noticeable. Neglecting the reverse (LS $\rightarrow$ HS) spontaneous relaxation and neglecting also the bulk absorption of light, the macroscopic master equation

of the system is written:

$$\frac{dn_{NS}}{dt} = \Phi_{up} - \Phi_{down} = I_0\omega(1 - n_{HS}) - n_{HS}k_\infty \exp\left(-\frac{E_a(0)}{kT}\right)\exp(-\alpha(T,x)n_{HS}) \quad (4)$$

where Φ_{up}, Φ_{down} are the n_{HS}-flows, from LS $\rightarrow$ HS and *vice versa*, respectively due to photo-excitation and relaxation. $I_0\omega$ is the probability per time unit for a LS molecule to switch to the HS state, with I_0 the beam intensity (in photons/s $\times$ cm^2) and ω a proportionality factor which includes the absorption cross-section of the optically active element. The steady state of the system (the state reached for time $\rightarrow$ infinity) occurs when Φ_{up}, Φ_{down} are equal to each other, so that:

$$n_{HS}k_\infty \exp\left(-\frac{E_a(0)}{kT}\right)\exp(-\alpha(T,x)n_{HS}) = I_0\omega(1 - n_{HS}). \quad (5)$$

A similar equation was proposed by Prigogine *et al.* [34] for the macroscopic master equation associated with the cooperative adsorption-desorption process of molecules on a surface.

The discussion of equations (4, 5) is illustrated in Figure 4. The steady state value(s) is (are) given by the intersect(s) of the curves associated with $\Phi_{up}(n_{HS})$, which is a straight line, and with $\Phi_{down}(n_{HS}) \approx n_{HS}\exp(-\alpha n_{HS})$, the shape of which crucially depends on the self-acceleration factor $\alpha(T,x)$. The number of possible intersects is governed by the value of $\alpha(T,x)$, as follows:

(i) $\alpha < \alpha_c = 4$, a single solution is obtained, which continuously varies as a function of $I_0\omega$ and T. The limiting value $\alpha_c = 4$ is easily derived analytically using the condition that the straight line Φ_{up} and the tangent to Φ_{down} at the inflexion point are superimposed.

(ii) $\alpha > \alpha_c$, a 3-state situation may occur, according to the slope of the straight line, *i.e.*, depending on the value of I_0. A 3-solution situation is shown in Figure 4a. The stable/unstable characters of the solutions are obviously governed by the competition between Φ_{up} and Φ_{down} as illustrated in Figure 4b. The steady states are denoted LSS, USS, HSS, standing for low-, unstable-, high-n_{HS}-values, respectively.

We focus on the possible bistability of the system, which results in the formation of thermal and optical hysteresis:

- an optical hysteresis loop (at T = constant) is obtained, by changing I_0 which governs the slope of the straight line Φ_{up} ;
- a thermal hysteresis loop (at I_0 = constant) is obtained as well. Upon temperature variation, the rapid variation of the term $\exp(-E_a(0)/kT)$ approximatively results in an enlargement of Φ_{down} on the vertical scale.

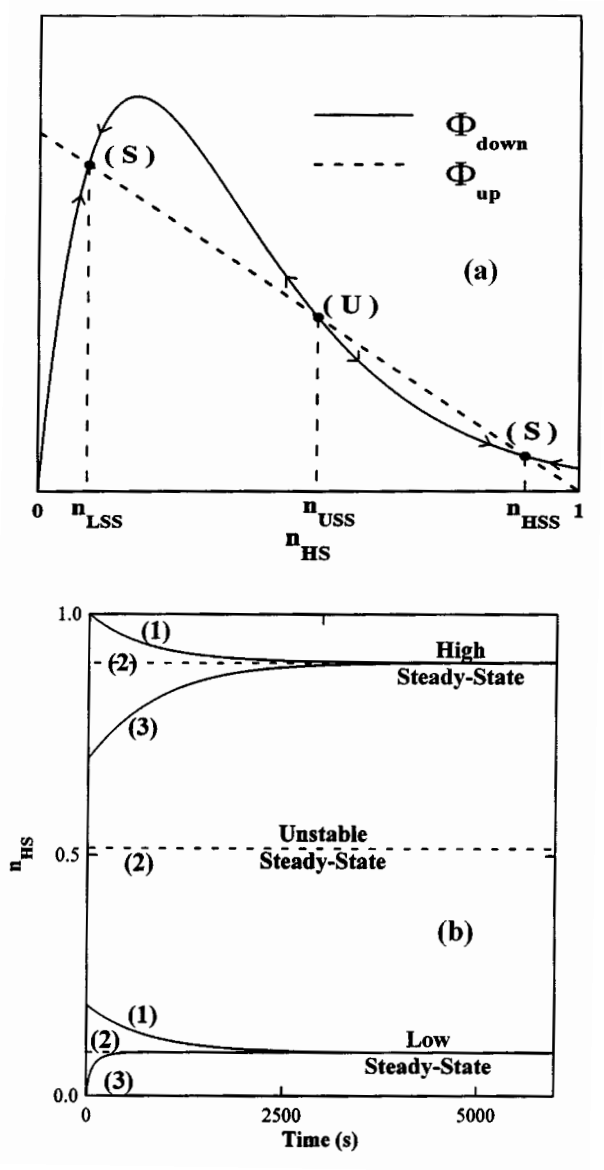

Fig. 4. Graphical investigation of equations (4, 5). The curves are computed using: $\alpha = 5.82$. (a) determination of the steady state values, as intersects of the curves; (b) time dependence of $n_{HS}(t)$, for different initial states.

These light-induced hysteresis effects can be denoted: LIOH/LITH (*i.e.* Light-Induced Optical/Thermal Hysteresis) in agreement with Kahn's and Letard's recent suggestion for the latter effect [35]. The hysteresis in the LIESST regime has been recently observed by Hinek *et al.* [36] on one of the two crystallographic sites of the system $[Fe(etz)_6](BF_4)_2$ (however not under continuous irradiation) and interpreted in terms of strong cooperative effects [36,37].

In the present work, we mainly aim to experimentally observe the bistability of the steady state, by varying the time, the temperature and the light intensity. In other words, we wish to obtain evidence for instability, and for steady states in form of thermal and optical hysteresis.

The convenient ranges of parameter values have been obtained semi-empirically, with the help of computations based on equation (5).

We also mention that introducing, in average, bulk absorption of light by LS molecules gives $\Phi_{up}(n_{LS})$, where $n_{LS} = 1-n_{HS}$, a form similar to that of $\Phi_{down}(n_{HS})$. Consequently bulk absorption may be an alternative source of bistability in thick samples. The physical description including bulk absorption would require accounting for the inhomogeneous character of the light flux, and this is beyond the scope of the present report.

4 Experimental results

$[Fe_xCo_{1-x}(btr)_2(NCS)_2]\cdot H_2O$ in the solid state has a planar polymeric structure [39] giving rise to a strong cooperativity for large x values. The synthesis, already described in [40] provides well shaped crystals. Pure iron crystals are rather transparent at room temperature (HS state) but turn to deep purple at low temperature (LS state); they unfortunately break when undergoing the LS $\rightarrow$ HS thermal transition. On increasing the Co content, the crystals at room temperature progressively change to yellowish, but turn to purple, as well, at low temperature. The solid solution has been previously studied [16,38,41] by magnetic measurements, calorimetry, Mössbauer spectroscopy and recently, reflectivity [14,16]. The pure iron system has a 24 K-wide thermal hystereses loop, around 130 K. On increasing the Co-content the hysteresis loop progressively narrows, and collapses at $x_c \approx 0.38$. The phase diagram of the solid solution (in $T-x$ axes) has been analysed and modelled in mean-field [38] and Monte-Carlo Metropolis computations [41] based on the Ising-like model. Some aspects of the photo-excitation at the lowest temperature have been described in [16], most important for here being (i) the onset of a relaxation in the tunneling regime, with a dependence on n_{HS} similar to that of the thermal relaxation; (ii) the observation that the LIESST experiments were successful in the diluted samples only. The mechanism which hinders the LIESST effect in the pure iron compound will be examined in Section 5.

Crystals of various iron contents were grown as described in [39]. We extensively studied 3 compositions, $x = 0.3$, 0.5, 0.85, in order to span the self-acceleration parameter below and above the critical value $\alpha_c = 4$. We prepared thin samples ($\leq$ 1 mg in a 3 mm inner diameter cell), with crystals very lightly crushed in order to obtain a flat filling of the magnetometer cell. This enhances the diffusion of the light in the sample (as confirmed by optical reflectivity measurements) and slightly contributes to the bulk attenuation of light intensity, in addition to the pure absorption effect. A standard 100 W tungsten halogen lamp fed by a variable voltage source (0−12 V), was used for illumination experiments, using an orange interferometric filter (100 nm-wide, centered at about 600 nm) the sample cell in the magnetometer received a power up to 60 mW/cm^2, measured ex-situ by a home-made bolometer. The power really entering the crystallites was assumed to be $\sim$ 80% of the power received by the cell. A more accurate determination of the ratio entering/received power would require a dedicated experiment, such as the measurement of the reversible magnetization jumps [42] observed when the light is switched on and off. Due to the present uncertainty, we shall neither try to estimate the quantum yield of the LIESST process, nor discuss the intensity values when comparing the data of different samples.

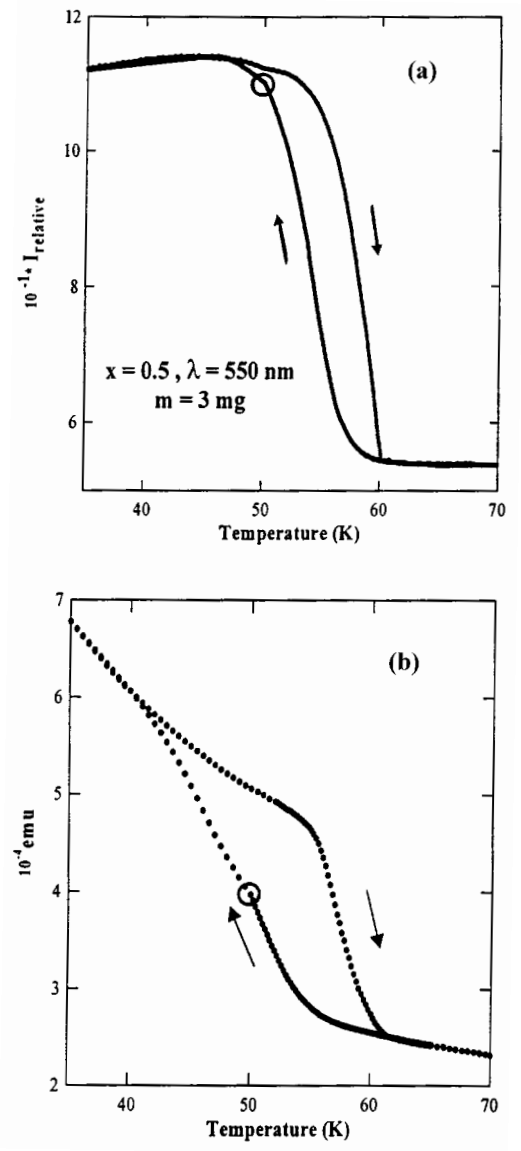

Fig. 5. Magnetic and optical responses for $x = 0.5$, $\lambda = 550$ nm, 40 mW/cm^2. (thick sample, 3 mg). Descending branch 0.2 K/2 min $\rightarrow$ 0.5 K/2 min, ascending 0.2 K/5 min $\rightarrow$ 0.5 K/5 min. The cycle is completed within 14 h.

We performed preliminary experiments on a $x = 0.5$, thick sample (3 mg) and soon changed to a thinner one (0.9 mg). In addition, we tried centered (550 nm) and shifted (600 nm) wavelengths. These experiments showed the large effect of bulk attenuation of light intensity on the magnetic signal, in comparison to the reflected signal which remained almost free from bulk attenuation effect,

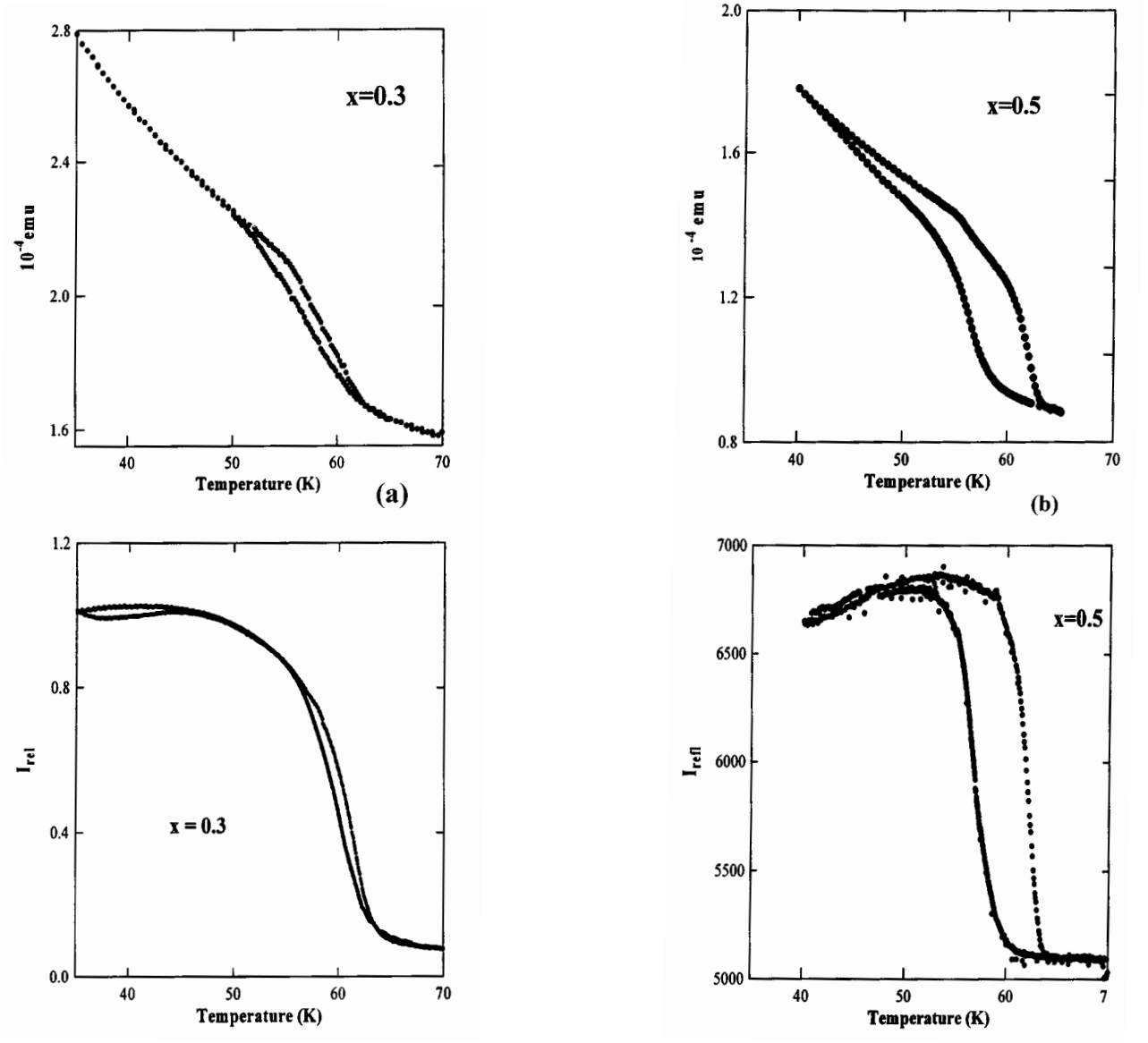

Fig. 6. Magnetic and optical responses for $x = 0.3$, 0.5, 0.85, $\lambda = 600$ nm, 40 mW/cm^2. Typical time to close the cycle is ~ 24 h.

since it detects the surface part of the sample. Typical distortions of the magnetic signal are shown in Figure 5: (i) a shift of the hysteresis loop towards lower temperatures (because light intensity is weaker in the bulk); (ii) enhancement of the low-temperature tail (the tail is mostly kinetic, due to the low value of the relaxation rate for large n_{HS} values). This kinetic character is demonstrated by a small feature (denote in Fig. 5 as a circle on each curve) which occurred upon an unexpected change in the programmed temperature sweep rate. This feature indicates that the steady state is not perfectly achieved.

Conclusive experiments were made on the thinner samples (1 mg), using a wavelength shifted at the edge of the $^1A_1 \rightarrow {}^1T_1$ absorption band (600 nm). The Light Induced Thermal Hysteresis loops, recorded by magnetic measurements and by optical reflectivity are shown in Figure 6. All compositions illustrate the advantage of optical detection, obviously free from bulk attenuation effects.

We have extracted n_{HS} values from the optical signals of Figure 6, assuming, as shown in Figure 1, a linear correlation between n_{HS} and the (relative) reflected intensity. The thermal loops, $n_{HS}(T)$, are shown in Figure 7, together with theoretical curves computed according to equation (5). For performing the computation, the molecular energy barrier values for $x = 0.3$ and 0.85 have been derived from the $x = 0.5$ value, according to the variation of the molar enthalpy change upon spin conversion, $\Delta H(x)$, in the solid solution. Data taken from [16] led to estimate $E_a(1/2) = 756$, 286 K for $x = 0.3$, 0.85, respectively. The α values which fit these thermal loops are such that $\alpha T = 160$, 275, 350 K, for $x = 0.3$, 0.5 and 0.85, respectively. These values are very close to those listed

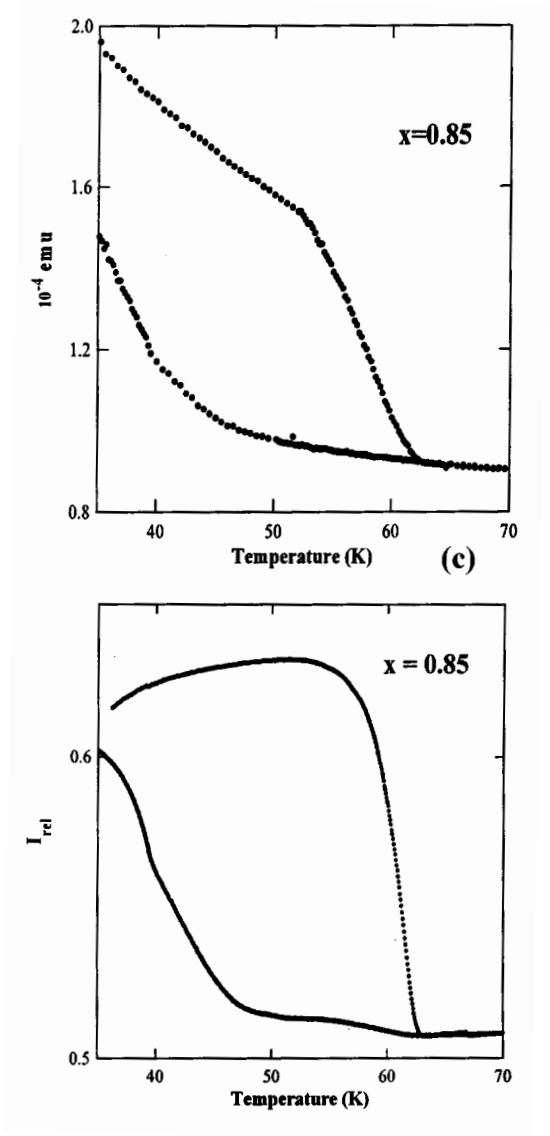

Fig. 6. (*Continued.*)

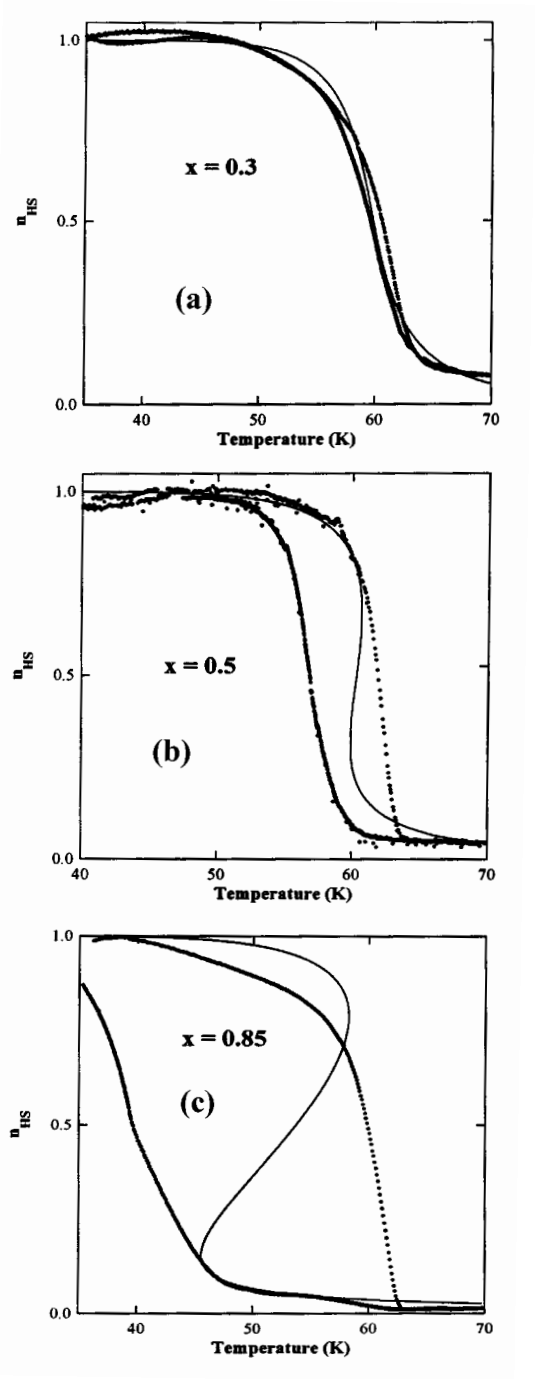

Fig. 7. Experimental n_{HS} data, derived from the optical curves of Figure 6. Solid lines are steady-state curves computed using equation (5). Fitted α-values are given in Table 1.

in Table 1, deduced from the corresponding relaxation curves. The general agreement obtained here with the model, for different compositions, corroborates the cooperative origin of the LITH effect.

To provide further experimental evidence for the bistability effect, free from kinetic effects, we have measured the time dependence of $n_{HS}(T)$, at constant temperature and light intensity, for the middle composition $x = 0.5$, at $T = 59$ and 60 K, after different thermo-optical histories of the sample. The 59 K curves are shown in Figure 8. The comparison to the expected behaviour, displayed in Figure 4b, reveals how complex is the bistability problem. Indeed, a range of steady state values was obtained. This gives evidence for a possible diphasic state of the system, *i.e.* for a demixtion process of the sample, into domains having the LSS and HSS values. Demixtion occurs when the thermo-optical history involves unstable situations. A pure steady state, *i.e.* a demixtion-free process, can be ensured when the thermo-optical history combines either high temperature and weak intensity, or low temperature and large intensity. Such are, in Figure 8, curve (a), pure low steady state, and curve (b), pure high steady state. A quantitative analysis, in terms of spinodal points, is developped in the next section.

To complete the investigation of the light-induced bistability, we have also observed the LIOH (optical) effect, on the same sample, at the constant temperature

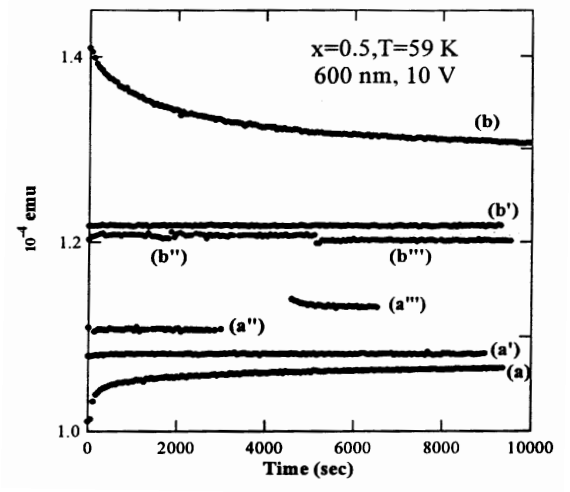

Fig. 8. Typical time dependances for $x = 0.5$, $T = 59$ K, $\lambda = 600$ nm, 40 mW/cm^2. (a) starting from the non-excited state (leading to pure low steady state), (b) starting from a low temperature saturated state (leading to pure high steady state) (a′, a″, a‴) follow (a) +1 hour at 58.5 K + 1 hour at 58 K + 10 min. at 50 mW/cm^2; (b′, b″, b‴) follow (b) +1 hour at 60 K +2 hours at 35 mW/cm^2 +2 h at 35 mW/cm^2.

of 58 K. The measurements are shown in Figure 9. The time dependence, for each value of light intensity, has been fitted by an exponential law, in order to determine the steady state value, which is reported in Figure 10 for each light intensity value, and form the expected LIOH loop. The shape of the loop was nicely reproduced by using equation (5), with a fitted value $\alpha T = 315$ K, in good agreement with the previous data.

5 Discussion

The presence of thermal and optical hysteresis effects in photo-excitable solids gives the thermo-optical history of the sample before any experiment, a crucial role, which can be referred to as the "thermo-optical treatment of the sample", in the discussion which follows.

Instability obviously leads to demixtion, *i.e.* to the transformation of the solid into a diphasic state from the optical and magnetical points of view. The kinetic aspects of demixtion are beyond the scope of the present study. We merely present, in Figure 11, time evolutions expected to be similar to those of Figure 8, excepted that temperature is slightly higher: 60 K instead of 59 K. The time evolutions have been recorded after different thermo-optical treatments. Curves (a,b) provide the position of the two stable steady states (LSS and HSS), both of them being sizeably below the 59 K values. Curves (c) show steady state values in-between the HSS and LSS values, typical for a biphased state of the sample. The particular shape of these curves provides further evidence for demixtion, since each of them results from the combination of curves going upwards (to the HSS state) and downwards (to the

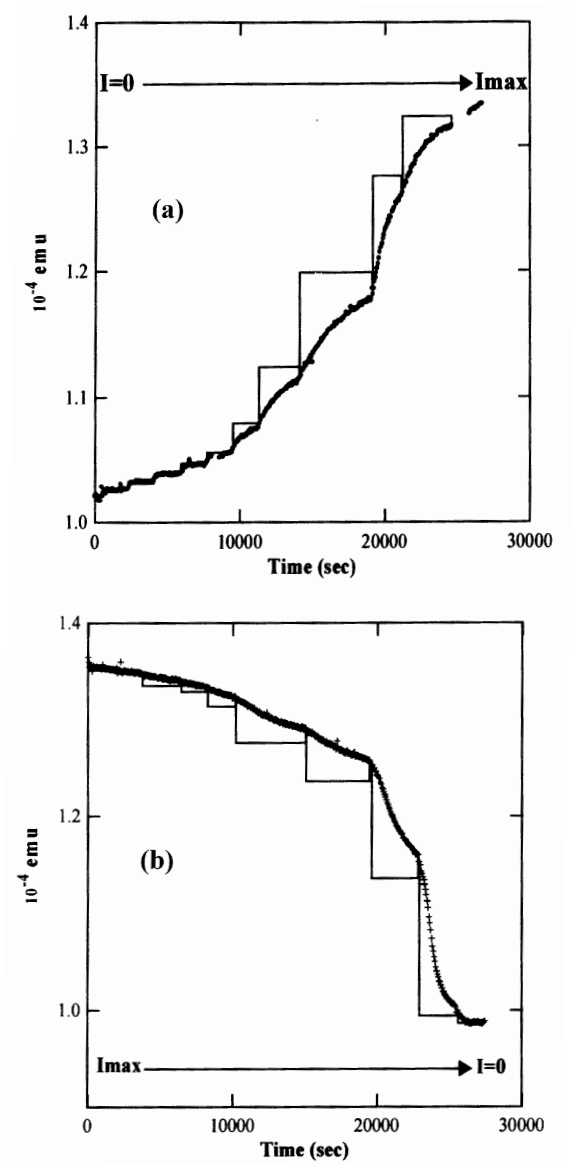

Fig. 9. Measurements for the light-induced optical hysteresis, with $x = 0.5$, $\lambda = 600$ nm, $T = 58$ K. The light intensity has been increased, then decreased by steps. For each step, the steady-state value has been estimated, by fitting an exponential law to the experimental time dependence. The successive steady state values are shown as a broken line.

LSS state) with different rates. Curve (d) displays a spurious behavior of the magnetic data which is not seen in the reflectivity curve, *i.e.* which only occurs in the bulk of the sample. At 59 K an unusual scatter of the magnetic data was already noticeable for several runs in the instability region.

Since the origin of the light-induced instability has been attributed to the cooperative character of relaxation, written in terms of a non-linear term in the macroscopic master equation (4), we have considered this non-linear term as the driving force for the enhancement of n_{HS} inhomogeneities in the sample. Such inhomogeneities can

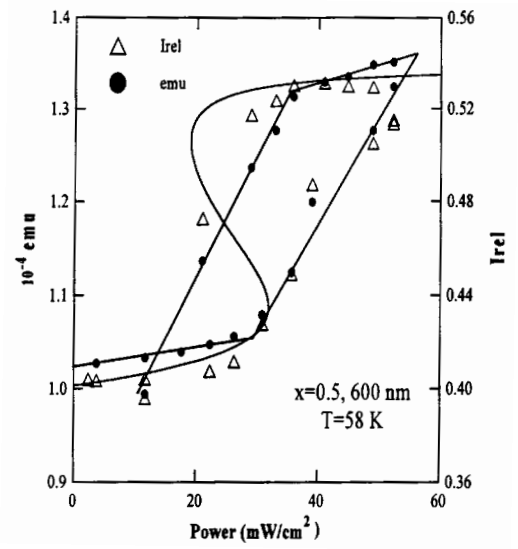

Fig. 10. Experimental light-induced optical hysteresis (LIOH) loop, from the steady-state values determined in Figure 9, using magnetic (circles) and optical (triangles) data. The full line is a computed curve using equation (5), with fitted value $\alpha T = 315$ K, so as to reproduce the width of the magnetic loop.

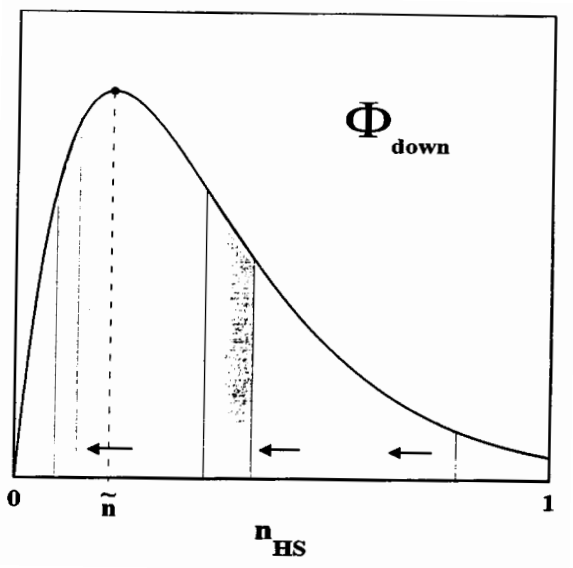

Fig. 12. The driving force for transient inhomogeneity, illustrated by a $\Phi_{down}(n_{HS})$ plot. An initial n_{HS}-distribution broadens till $\tilde{n}_{HS}$, because of a dispersive effect: the smaller n_{HS}, the larger the flux Φ_{down}, *i.e.* the velocity dn_{HS}/dt.

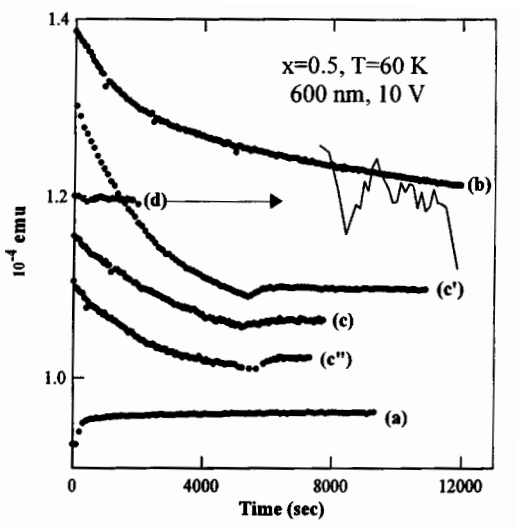

Fig. 11. Experimental n_{HS} time dependances, for $x = 0.5$, 600 nm, 40 mW/cm^2, 60 K. Initial states were: (a) non-excited state; (b) HSS state at larger intensity (but same temperature); (c, d) low-temperature non-saturated states.

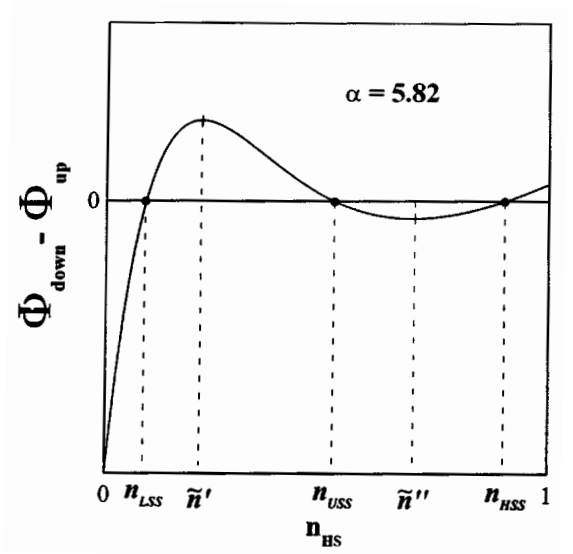

Fig. 13. Spinodal points, $\tilde{n}$, $\tilde{n}''$, limiting the range of values for which the system is unstable with respect to n_{HS} fluctuations.

occur spontaneously, due to the thermal fluctuations. The inhomogeneous trend is explained by the n_{HS} dependence of Φ_{down}, which is plotted in Figure 12: n_{HS}-fluctuations are thermally instable for $n_{HS} > \tilde{n}_{HS}$, value for which $\Phi_{down}(n_{HS})$ is at maximum. For $0 < n_{HS} < \tilde{n}_{HS}$, the system is stable with respect to n_{HS} fluctuations. Then n_{HS} inhomogeneities may be expected to transiently increase. This transient instability vanishes below the threshold value $\tilde{\alpha}_c = 1$ (such that $\tilde{n}_{HS} = 1$). The occurrence of inhomogeneities during the relaxation process results in a $n_{HS}(t)$ curve which is an envelop of sigmoidal curves, and contributes to the tail observed in the curves of Figure 3. A quantitative analysis of experimental data will be presented in a separate paper.

In presence of light, the same analysis holds, and two spinodal points appear, as shown in Figure 13. Thus, the theoretical curves predicting the thermal or optical dependances of the steady states (LITH, LIOH curves) should be completed by spinodal limiting curves. This will be considered in a further work, from both theoretical and experimental viewpoints.

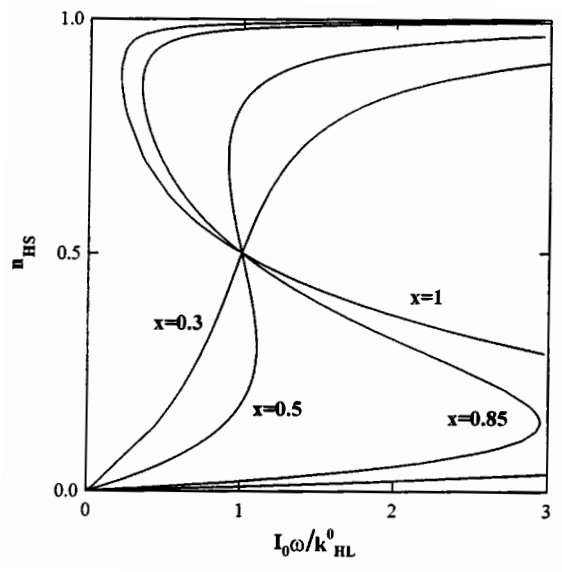

Fig. 14. Computed curves for the intensity threshold effect, following equations (6, 7), plotted as a function of $I_0\omega/k_{HL}(n_{HS} = 1/2)$, with $\alpha_0(x = 0.5) = 4.7$.

Another consequence of the non-linear term in equations (4, 5) is the occurrence of an intensity threshold in cooperative solids. Indeed, relaxation occurs even at low temperature, for which LIESST is usually carried out. The tunnelling regime is sensitive to the cooperative effect which modulates the energy barrier. The macroscopic master equation is then written:

$$\frac{dn_{HS}}{dt} = -n_{HS}k_\infty(n_{HS} = 0)\exp(-\alpha_0 n_{HS}) + I_0\omega(1 - n_{HS}). \quad (6)$$

Equation (6) is quite similar to the previous equation (4), except for temperature, and similarly leads to the light-induced instability and hysteresis. The self-acceleration factor α_0, similarly originates from cooperativity. In diluted system, mean-field approach, the analogy with equation (3) holds, so that:

$$\alpha_0(x) = A_0 x. \quad (7)$$

Since the goal of quantitative LIESST is to reach the high steady state, it is clear that light-induced optical hysteresis has the effect of an intensity threshold. Of major importance is the fact that the threshold value dramatically increases on increasing the cooperativity parameter. This is illustrated in Figure 14. Thus, strongly cooperative materials may even miss the initial energy barrier needed to provide the excited state a sufficient lifetime; the barrier has to be induced by the population of the excited state. This explains, at least qualitatively, why the LIESST is almost unefficient for the pure $[Fe(btr)_2(NCS)_2] \cdot H_2O$ solid, while the light excitation is relatively easy for the diluted compounds.

As a further consequence of light-induced instabilities, the onset of patterns, spin-domain like, can be predicted. The photographs of single crystals during relaxation which follows the locally induced LIESST confirm this hypothesis and will be presented in a separate paper. Optical microscopy studies should be carried out on single crystals under permanent irradiation. Both steady-state and transient patterns are expected, with possible periodic and chaotic behaviours.

It is worth noting that a detailed investigation of the kinetics of the LIESST process in cooperative systems has yet to be done. Experiments similar to those presented here, in the steady state, should provide the required information on the relaxation process. Further investigation of the LIESST effect might address the basic question of cooperative effects in the excitation process itself. So far, the question is not clearly answered: (i) the present data agree quite well with a linear, *i.e.* non-cooperative, excitation term; (ii) on the other hand, some evidence for a cooperative photo-induced phase transition was recently reported for a $[Fe^{II}(2\text{-pic})_3]Cl_2 \cdot EtOH$ single crystal under intense laser excitation [43]. The very fast kinetics of the latter experiment seems to rule out the indirect mechanism of cooperative relaxation which is efficient here. Thus, cooperative excitation in spin-crossover solids remains an interesting open problem.

6 Conclusion

In addition to the exciting aspects of light-induced bistability, which is novel for cooperative spin-crossover solids, we stress the transient inhomogeneous character of relaxation, which occurs as soon as $\alpha > 1$, *i.e.* far below the occurence of the thermal entropy-driven transition which usually characterizes cooperative systems. The inhomogeneous character has to be accounted for as an additional parameter in relaxation models. The present analysis also helps to understand how the LIESST process is severely hindered by cooperativity.

No doubt light-induced bistability, which is a feature inherent to cooperative bistable systems, will give rise to spectacular patterns in materials under continuous excitation.

Aknowledgements are due to A. Wack and P. Renaudin for technical assitance, A. Hauser, H. Spiering, R. Lapouyade and S. Koshihara for valuable discussions, O. Kahn and J.F. Letard for communicating their results before publication, J. Hodges for pre-reading of the manuscript, Swiss National Science Foundation for a post-doctotal grant (J.J) and EEC/TMR program for financial support (Contract TOSS, ERB-FMRX-CT98-0199).

References

1. P. Gütlich, Struct. Bonding (Berlin) **44**, 83 (1981).
2. H. Toftlund, Coord. Chem. Rev **94**, 67 (1989).
3. E. König, Struct. Bonding (Berlin) **76**, 51 (1991).

4. a) O. Kahn, *Molecular Magnetism* (VCH, New-York, 1993); b) O. Kahn, Cur. Op. Solid State & Materials Science **1**, 547 (1996).
5. J. Zarembowitch, O. Kahn, New J. Chem. **15**, 181 (1991).
6. a) O. Kahn, J. Kröber, C. Jay, Adv. Mat. **4**, 718 (1992); b) O. Kahn, C. Jay-Martinez, Science **279**, 44 (1998).
7. S. Decurtins, P. Gütlich, C.P. Köhler, H. Spiering, A. Hauser, Chem. Phys. Lett. **1**, 139 (1984).
8. P. Gütlich, A. Hauser, H. Spiering, Angew. Chem. Int. Ed. Engl. **33**, 2024 (1994).
9. A. Hauser, Comments Inorg. Chem. **17**, 17 (1995).
10. A. Hauser, Coord. Chem. Rev., 11, 275 (1991).
11. J. Krober, J.P. Audière, R. Claude, O. Kahn, J. Haasnoot, F. Grolière, C. Jay, A. Bousseksou, J. Linares, F. Varret, A. Gonthier-Vassal, Chem. Mater. **6**, 1404 (1994).
12. O. Kahn, E. Codjovi, Phil. Trans. R. Soc. London A **354**, 359 (1996).
13. E. Codjovi, L. Sommier, O. Kahn, C. Jay, New J. Chem. **20**, 503 (1996).
14. W. Morscheidt, J. Jeftic, E. Codjovi, J. Linares, A. Bousseksou, H. Constant-Machado, F. Varret, Measurement Science and Technology **9**, 1311 (1998).
15. F. Varret, H. Constant-Machado, J.L. Dormann, A. Goujon, J. Jeftic, M. Noguès, A. Bousseksou, S. Klokishner, A. Dolbecq, M. Verdaguer, *Proceedings of ICAME'97 (Intern. Conf. Applications Mössbauer Effect, Rio de Janeiro Brésil, Sept.1997)*, to appear in Hyperfine Interactions.
16. H. Constant-Machado, Ph.D. thesis, University of Paris VI, France (1997).
17. J. Jeftic, A. Hauser, Chem. Phys. Lett. **248**, 458 (1996).
18. H. Spiering, E. Meissner, H. Köppen, E.W. Müller, P. Gütlich, Chem. Phys. **68**, 65 (1982).
19. A. Hauser, P. Gütlich, H. Spiering, Inorg. Chem. **25**, 4345 (1986).
20. A. Hauser, J. Chem. Phys. **94**, 2741 (1991).
21. J. Jeftic, A. Hauser, J. Phys. Chem. B **101**, 10262 (1997).
22. A Bousseksou, Ph.D. thesis, University of Paris VI, France (1992).
23. A. Bousseksou, J. Nasser, J. Linares, K. Boukheddaden, F. Varret, J. Mol. Cryst. Liq. Cryst. **234**, 269 (1993).
24. A. Bousseksou, F. Varret, J. Nasser, J. Phys. I France **3**, 1463 (1993).
25. A. Bousseksou, H. Constant-Machado, F. Varret, J. Phys. I France **5**, 747 (1995).
26. C.P. Slichter, H.G. Drickamer, J. Chem. Phys. **56**, 2142 (1972).
27. H.G. Drickamer, C.W. Frank, *Electronic Transitions and the High Pressure Chemistry and Physics of Solids* (Chapman and Hall, London, 1973).
28. P. Adler, L. Wiehl, C.P. Köhler, H. Spiering, P. Gütlich, J. Phys. Chem. Solids **48**, 517 (1987).
29. J. Jeftic, H. Romstedt, A. Hauser, J. Phys. Chem. Solids **57**, 1743 (1996).
30. J. Jeftic, R. Hinek, S.C. Capelli, A. Hauser, Inorg. Chem. **36**, 3080 (1997).
31. N. Willenbacher, H. Spiering, J. Phys. C: Solid State Phys. **21**, 1423 (1988).
32. H. Spiering, N. Willenbacher, J. Phys.-Cond. **1**, 10089 (1989).
33. A. Hauser, H. Romstedt, H. Spiering, results presented on the *3rd Spin Crossover Family Meeting*, Seeheim/Germany, 1998.
34. I. Prigogine, R. Lefever, J.S. Turner, J.W. Turner, Phys. Lett. A **51**, 317 (1975).
35. J.F. Letard, O. Kahn, private communication.
36. R. Hinek, H. Spiering, P. Gütlich, A. Hauser, Chem. Eur. J. **35**, 1435 (1997).
37. A. Hauser, J. Jeftic, H. Romstedt, R. Hinek, Mol. Cryst. Liq. Cryst. **286**, 217 (1996).
38. J.P. Martin, J. Zarembowitch, A. Bousseksou, A. Dworkin, J.G. Haasnoot, F. Varret, Inorg. Chem. **33**, 6325 (1994).
39. W. Vreugdenhil, S. Gorter, J.G. Haasnoot, J. Reedijk, Polyhedron **4**, 1769 (1985).
40. J.G. Haasnoot, W.L. Groeneveld, Z. Naturforschung **34b**, 1500 (1979).
41. H. Constant-Machado, J. Linares, F. Varret, J.G. Haasnoot, J.P. Martin, J. Zarembowitch, A. Dworkin, A. Bousseksou, J. Phys. I France **6**, 1203 (1996).
42. F. Varret, M. Noguès, J.L. Dormann, E. Dujardin, T. Mallah, M. Verdaguer, in preparation for Eur. Phys. J. B.
43. A. Mino, Y. Ogawa, S. Koshihara, Mol. Cryst. Liq. Cryst., to appear.